Hindawi
Geofluids
Volume 2022, Article ID 7743490, 19 pages
https://doi.org/10.1155/2022/7743490

Research Article

Study on Energy Density Distribution and Mass Fractal of Deep Saturated Coal Samples under Uniaxial Stepwise High Stressed Loading and Unloading Path

Xiaoyu Chen,[1,2] **Qiangling Yao**,[1,2] **Changhao Shan**,[1,2] **Liqiang Yu**,[1,2] **Liang Chen**,[1,2] **Qiang Xu**,[1,2] **Ze Xia**,[1,2] **and Liu Zhu**[1,2]

[1]*School of Mines, State Key Laboratory of Coal Resources and Safe Mining (CUMT), China University of Mining & Technology, Xuzhou 221116, China*
[2]*School of Mines, China University of Mining & Technology, Xuzhou 221116, China*

Correspondence should be addressed to Qiangling Yao; yaoqiangling@cumt.edu.cn

Received 20 May 2022; Revised 12 August 2022; Accepted 2 September 2022; Published 16 September 2022

Academic Editor: Zhenlong Song

The geostress in deep coal roadway is high and affected by mining frequently; under the influence of water-rock interaction, the bearing capacity of coal continues to deteriorate. Based on the characteristics of short water absorption process and low moisture content of deep coal samples in this experiment, the threshold range of quantitative division of water absorption stage of coal samples is given, and the structural characteristics of deep coal samples that are more susceptible to cracks are analyzed. The actual loading process is simulated through uniaxial stepwise high stressed loading and unloading experiments, the gradual development of cracks was the root cause of instability of coal, and saturated water mainly aggravates the instability process through these cracks; the stepwise high stressed loading and unloading path makes cracks more likely to occur in the sample. After each level of loading and unloading, the average stiffness is approximately linear trend degradation. By calculating the energy density of deep coal samples in each stage before the peak, the change of energy density indexes between saturated and dried samples is different from relative shallow samples, and the energy density indexes do not decrease but increases instead. However, the proportion of each energy is generally positive and inverted "U"-type distribution. The change trend of plastic energy in proportion to dissipation energy can be used as the judgment feature of coal sample instability. The instability of deep coal samples is mainly caused by the gradual dissipation of plastic energy to generate cracks and divided into fragments with large and long edge, resulting in low mass fractal dimension. In engineering practice, the loading times should be reduced and the suitable pressure grouting should be conducted timely to delay the deterioration process of crack development in deep water-bearing coal under high stress disturbance.

1. Introduction

Deep mining is often in the complex environment of high geostress, high karst water pressure and strong mining disturbance [1–4]. While the coal in the roadway is bearing deep high stress, it is also affected by the repeated disturbance of coal seam group mining and surrounding mining activities [5–8] so that the internal cracks and damage continue to develop under the stress path of cyclic loading and unloading [9–11], resulting in frequent failure of anchor bolt or cable and continuous degrade of structural stability [10, 12, 13]. Relevant studies [14, 15] also show that the strength characteristics and deformation law of coal (rock) under cyclic loading and unloading path are significantly different from bearing characteristics of coal (rock) under uniaxial compression path. Under the conditions of coal seam water injection [16], water-retaining mining [17], coal and gas comining [18], the water content in the cracks around the coal body will increase. When water enters the coal body, the friction coefficient among mineral particles will be reduced, and the relative sliding difficulty of the crack surface will be

reduced [19]. Therefore, after the coal is subjected to cyclic loading that is under the water-rock interaction environment for a long time, the mechanical properties will further change [20], resulting in the bearing characteristics of the deep coal body near the roadway in a certain range similar to the one-dimensional loading state [21] continue to deteriorate and even affect the normal mining activities. Therefore, it is necessary to carry out the research on the bearing characteristics of deep water-bearing coal under uniaxial stepwise high stressed loading and unloading path.

At the same time, in the process of loading and instability of coal (rock) body, energy conversion will be accompanied. Pu discussed the evolution law of prepeak energy accumulation and dissipation of red sandstone specimens under uniaxial cyclic loading and unloading path [22]; Wang analyzed the energy conversion mechanism of sandstone specimen failure under uniaxial cyclic loading and unloading path [23]. The unloading test of Jia showed that the elastic energy, input energy, and dissipation energy increased with the increase of depth [24]. The study of Wang on triaxial cyclic loading and unloading of deep coal showed that macroscopic cracks are produced by plastic energy on the input energy of specimens, resulting in irreversible damage to the coal body [25]. Meng found that the loading energy consumption ratio of limestone under triaxial cyclic loading-unloading path can characterize the accumulation state of internal crack damage [26]. Xue studied the energy evolution characteristics of coal under different gas pressures in deep underground engineering environment [27]. With the continuous input and dissipation of energy, the coal body eventually destroyed and produced a number of fragments with different particle sizes. However, due to the different loading environment and its own structure, the size distribution characteristics and mass fractal dimension of these fragments are different, which somehow reflects the instability process of the specimen. Among them, Tang [28] carried out the study on the mass fractal law of coal samples with relatively shallow burial depth affected by different soaking times under uniaxial compression path. Li [29] studied the mass fractal law of coal samples with relatively shallow burial depth affected by different loading rates under stepwise loading and unloading paths. Duan [30] studied the mass fractal law of coal samples with relatively shallow burial depth affected by different periodic loads under uniaxial compression paths. In the above research [28–30], the energy density of coal samples with relatively shallow burial depth is larger than the deep, and the mass fractal dimension is between 1.92 and 2.34, mainly generating small side length fragments and particles.

Although previous studies have made a detailed summary and analysis of bearing characteristics, energy distribution, and mass fractal of the nondeep coal, there are few experimental studies on deep coal under the condition of "saturated-uniaxial stepwise high stressed loading and unloading." Therefore, in order to grasp the bearing characteristics of coal in deep high stress and water-rich roadway better, find out the main control factors affecting the bearing stability of deep coal mass. This paper carried out uniaxial high stress compression test under stepwise loading and unloading path and related verification work on deep saturated coal samples. To some extent, the water absorption law, bearing performance, energy distribution, and mass fractal characteristics of coal in deep high stress and water-rich roadway are obtained, which has guiding significance of some engineering and some reference significance of similar research.

2. Material Preparation and Experimental Methods

2.1. Specimen Preparation. The coal samples are taken from 11-2 coal seam of Zhujixi Coal Mine in Huainan City, Anhui Province. The occurrence depth is 962-1039 meters, which is in line [31] with the general concept of 700-1000 meters as the depth of deep coal mine proposed by Chinese academia. According to the requirements [32–35] of the test procedures of physical and mechanical properties of rock, coal samples were processed into $50 * 50 * 100$ mm cuboid specimens and then selected 12 coal samples and divided them into A, B, C, and D groups with no obvious cracks and no obvious differences in appearance, quality, and size. Group A is the grouping of drying specimens under uniaxial compression stress path. Group B is the grouping of drying specimens under uniaxial stepwise high stressed loading and unloading path. Group C is the grouping of saturated specimens under uniaxial compression stress path. Group D is the grouping of saturated specimens under uniaxial stepwise high stressed loading and unloading path.

2.2. Water Immersion Experiment and Wave Velocity Detection of Deep Coal Samples. According to the requirements of the regulations [32], the deep coal samples were dried and weighed and the quality data recorded. Then, the samples were immersed in water block by block to absorb the water. At the early stage, the quality changes were recorded every hour and every 4-8 hours in the late stage. When the recorded quality was unchanged, the state was defaulted to the reached saturation.

The wave velocity information of deep coal specimens was tested by HS-YS301T rock acoustic parameter tester. The average wave velocity of saturated coal samples was 2.016 km/s, and the standard deviation was 0.21. The average wave velocity of drying coal sample is 1.063 km/s, the standard deviation is 0.08, the dispersion is small, and the concentration is high, which ensured the rationality of specimen selection.

2.3. Loading Scheme. The MTS-C64.106 electronic-hydraulic servo universal testing machine of the State Key Laboratory of Coal Resources and Safe Mining (CUMT) was used to conduct uniaxial compression test and uniaxial stepwise high stressed loading and unloading experiment on drying and saturated deep coal specimens. Firstly, the uniaxial compression experiment was carried out, and the average value of uniaxial failure load of specimens was about 20 kN. According to the strength results of uniaxial compression test, the loading path of coal in deep roadway is simulated by uniaxial stepwise high stressed loading and unloading. Approximately 25% load value of the average peak uniaxial compression is used as the threshold value of coal samples from the crack compaction stage to the crack development stage [19] to simulate the basal

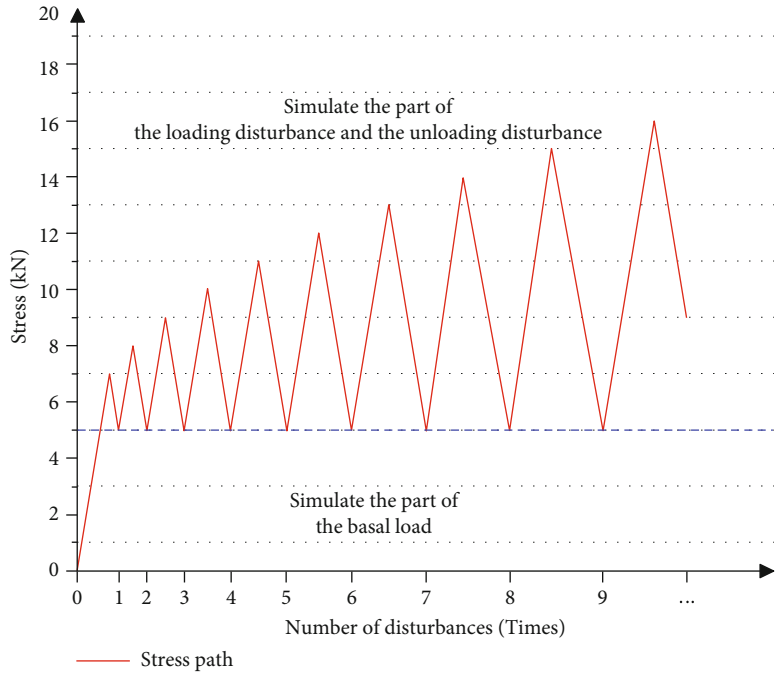

Figure 1: Diagram of the loading and unloading path.

load part of deep coal samples. So according to the path of 0-5-7-5-8-5-...kN to loading and unloading step by step until the specimen destroyed, the loading path is shown in Figure 1.

3. Results and Discussion

3.1. Quantitative Division of Threshold Range in Water Absorption Stage of Coal Samples. In this experiment, the average saturated moisture content of deep coal samples is about 1.25%, and the moisture content is low, as shown in Figure 2.

Combined with the experimental results, the moisture content-time fitting formula of coal samples with relatively shallow burial depth in References [28, 36–38] was used to draw the images of the average experimental moisture content in the first 40 hours of different coal samples, as shown in Figure 3.

It can be seen from References [28, 36–38] that the saturated water absorption stage of coal samples is sequentially within 24-40 hours, 20-40 hours, 24-40 hours, and 24-40 hours in the later immersion stage of relatively shallow buried depth specimens in Figure 3. The deep coal samples in the later immersion stage in the 8-40 hours of this experiment, the average rising rates of moisture content of each coal sample are 0.06%/h, 0.05%/h, 0.03%/h, 0.03%/h, and 0.01%/h, respectively. However, the calculation of relative water absorption rising rate in each stage showed that the relative rising rates of water absorption to total water absorption in each coal sample stage were 0.56%/h, 0.55%/h, 0.63%/h, 0.53%/h, and 0.51%/h, and the data dispersion was low. The calculation formula of relative water absorption rate is as follows:

$$R_r = \frac{W_s}{W \cdot t_s}. \quad (1)$$

In the formula, R_r is the relative water absorption rising rate, W_s is the absorbing water ratio in each stage, W is the absorbing water ratio of the whole procession, and t_s is the time consumed of each stage.

In previous studies, the classification criteria of the three water absorption stages were not given clearly and quantitatively. Generally, they were artificially divided according to the trend of the moisture content-time curve. Therefore, based on the calculation value of the average rising rate of the ratio of the stage water absorption of the five groups of coal samples to the total water absorption of the whole process, the threshold range of the relative water absorption rate of the saturated water absorption stage of the coal sample was uniformly defined as 0-1%/h, as shown in Figure 4. According to the above analysis, the corresponding reference thresholds were defined as 1-5%/h and 5-100%/h for the slow and rapid water absorption stages.

3.2. Water Absorption and Structural Characteristics of Deep Coal Samples

(1) It can be seen from Figure 3 that the total water absorption and absolute water absorption rate of this deep coal sample are at a low level compared with those of the coal sample with relatively shallow burial depth. Previous studies [19, 28, 36–39] show that the water moves first in cracks and big pores and then moves in smaller pores. Before mining space formed, under the condition of deep high confining pressure, the pores of deep coal body are compacted after a long geological process to produce irreversible plastic deformation. The bigger confining pressure is, the higher degree of pore compaction

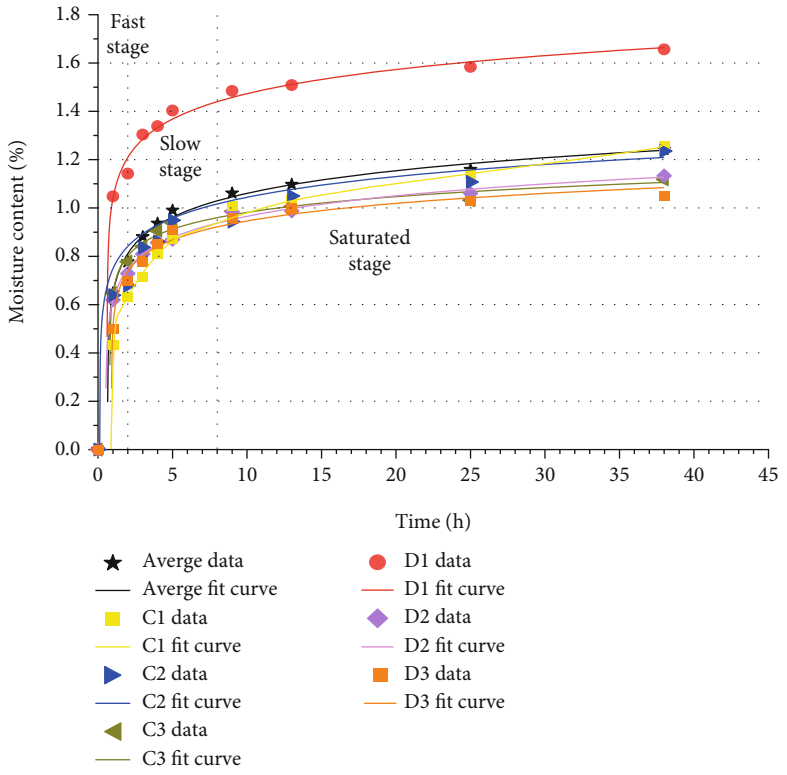

Figure 2: Relationship between time and moisture content of deep coal sample.

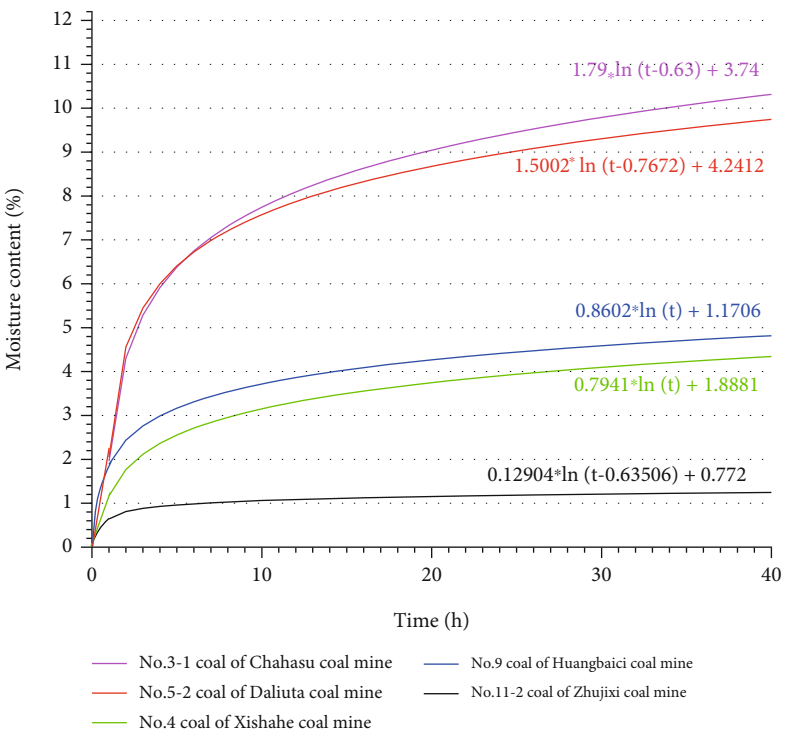

Figure 3: Relationship between time and moisture content of coal samples.

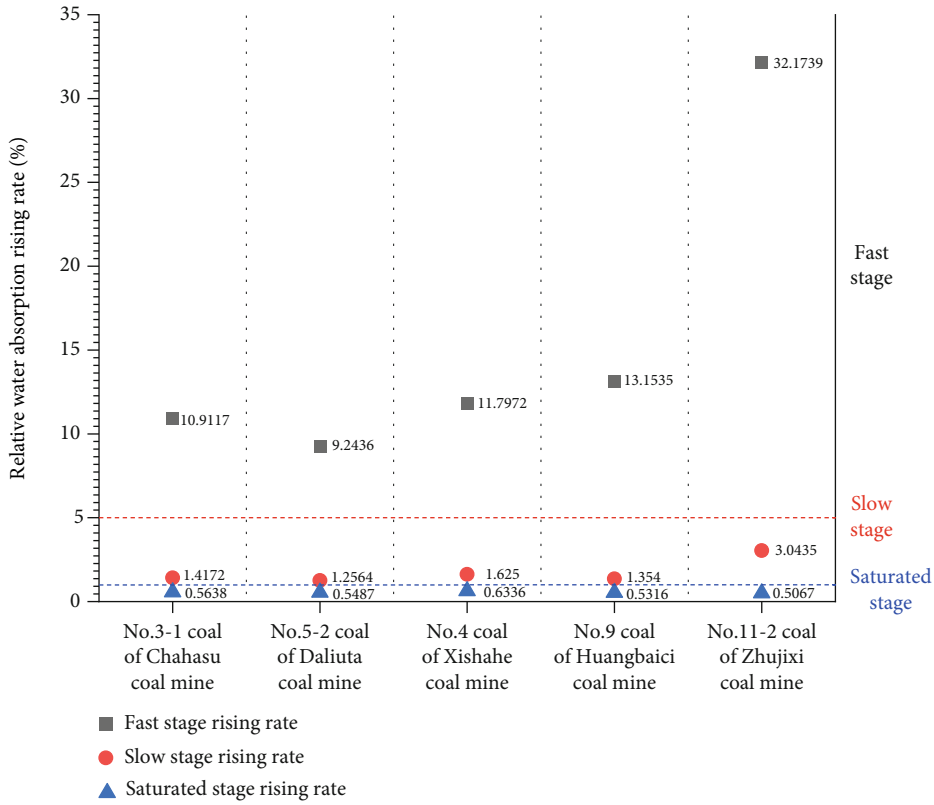

Figure 4: Relative water absorption rate of threshold stage.

in the coal skeleton is and the larger compact volume is. The total volume of pore (V_p), the total cross-sectional area of pore (S_p), and the number of cracks will decrease permanently compared with shallow coal before excavation. In the process of mining, with the gradual weakening and dissolution of confining pressure, cracks with a certain volume and scale will be formed in coal [40], as shown in Table 1. When we select the specimens of mechanical experiments, the specimens with obvious macroscopic cracks are often excluded. So, the total volume of cracks (V_c), the surface area of cracks (S_c), and the number of cracks (N_c) of deep coal samples used in the experiment will be reduced compared with actual deep coal body. Elimination of the larger macroscopic crack makes V_c and S_c generally at a low level in meso- and microlevels. And due to the porous medium characteristics [41] of coal, the total volume of pore (V_p) accounts for the vast majority of the total volume of water absorption at the macroscopic level. Combined with the above analysis, the relationship in the specimen can be deduced as $V_{c\text{-shallow}} < V_{c\text{-deep}} << V_{p\text{-deep}} < V_{p\text{-shallow}}$, and then, the relationship of water storage volume between deep coal specimen and relative shallow specimen can be obtained as $V_{c\text{-deep}} + V_{p\text{-deep}} < V_{c\text{-shallow}} + V_{p\text{-shallow}}$. Therefore, the total water absorption of deep coal samples will be less than that of shallow coal samples after removing the influence of hydrophilic substances. Similarly, the relationship between $S_{c\text{-shallow}} < S_{c\text{-deep}} << S_{p\text{-deep}} < S_{p\text{-shallow}}$ can be deduced, and then, the relationship of cross-sectional area of water absorption can be obtained as $S_{c\text{-deep}} + S_{p\text{-deep}} < S_{c\text{-shallow}} + S_{p\text{–shallow}}$. Therefore, the total water absorption of deep samples will be less than the total water absorption of coal samples with relatively shallow buried depth in the same period

Table 1: Reference range of scales with the crack.

Type of cracks	Macroscopic	Mesoscopic	Microscopic
Reference range (m)	10^{-3}	10^{-3}-10^{-7}	10^{-7}

(2) It can be seen from Figures 3 and 4 that the duration of the rising stage of water absorption of deep coal samples is shorter, and the relative water absorption efficiency is higher than the coal samples with relatively shallow buried. Combined with the analysis of the previous section, after having a certain free space, the high confining pressure release of deep coal samples will form more crack channel of water ($N_{c\text{-deep}}$) and larger cross-sectional area of crack channel ($S_{c\text{-deep}}$) than the coal sample with relatively shallow buried, and these data are positively correlated with water absorption efficiency. While the total water absorption of deep samples is lower than the coal sample with relatively shallow buried, and

Figure 5: Elimination of coal sample in mechanical experiment.

this data is negatively correlated with water absorption efficiency, so the relative water absorption efficiency of deep coal samples is higher

(3) The moisture content and water absorption rate of deep coal in the actual mining face will be significantly higher than those of the experimental specimen. The moisture content and water absorption rate of deep coal body in the actual roadway will be significantly higher than those of the experimental specimen. Once the deep coal is excavated, the disturbance of loading and unloading caused by the space-time and dynamic relationship of mining, there will be more volume of cracks (V_c) and more cross-sectional area (S_c), and there will not be a process of removing specimens with obvious macroscopic and microscopic cracks. As is shown in Figure 5, the specimens with obvious macroscopic cracks were selected from the eliminated products during the preparation of specimens; the saturated moisture content, the absolute water absorption rate in the fast stage, and the uniaxial compressive strength were 4.05%, 1.67%/h, 0.94 MPa and 5.6%, 2.62%/h, 1.07 MPa, respectively. Compared with the experimental specimens, these specimens showed higher moisture content, faster water absorption rate, and extreme lower uniaxial compressive strength. Therefore, combined with the above analysis, it can be seen that the deep coal samples have denser pore skeleton and are more easily controlled by cracks than the coal samples with relatively shallow buried

3.3. Wave Velocity Detection and Analysis Verification of Deep Coal Samples. Wave velocity detection can reflect changes in microstructure of samples in somewhat [42]. Comparing the wave velocity test information of coal sample with shallow buried depth [28] and drawing Figure 6 for analysis, the wave velocity dispersion of deep saturated coal sample is bigger than that of deep drying coal sample. It shows that water not only fills the internal cracks and pores of the coal sample but also increases the internal uniformity of a specimen. At the same time, it also plays a role in amplifying the difference of wave velocity between different specimens. The wave velocity increases significantly of the coal sample with less cracks after filling with relatively small amount of water. However, due to the large amount of internal cracks of the coal samples with poor integrity, the absolute amplitude of wave velocity increase after water filling is less than that of coal sample with good initial structural integrity.

It can be seen from the analysis in Section 3.2 that the quantity and volume of internal cracks in deep coal specimen under drying state are more than those in the specimen in the relatively shallow buried, so the electromagnetic wave propagation is slow. However, the pore skeleton density of deep coal is higher, and the electromagnetic wave propagates faster in the solid-skeleton area than that in the specimen in the relatively shallow buried. However, after saturated immersion, the average wave velocity of the deep coal sample filled with crack is larger than that of the nondeep coal samples filled with more pores. Therefore, it can be considered that the degree of crack development plays a major control role. This conclusion is also reflected in the eliminated specimens with obvious macroscopic and microscopic cracks in Figure 5. The wave velocity is only 0.579 km/s and 0.630 km/s, which verifies the view that deep coal samples are more susceptible control and influence due to cracks.

3.4. Analysis and Discussion on Bearing Characteristics of Deep Coal Samples. The stress-strain curves of deep coal samples

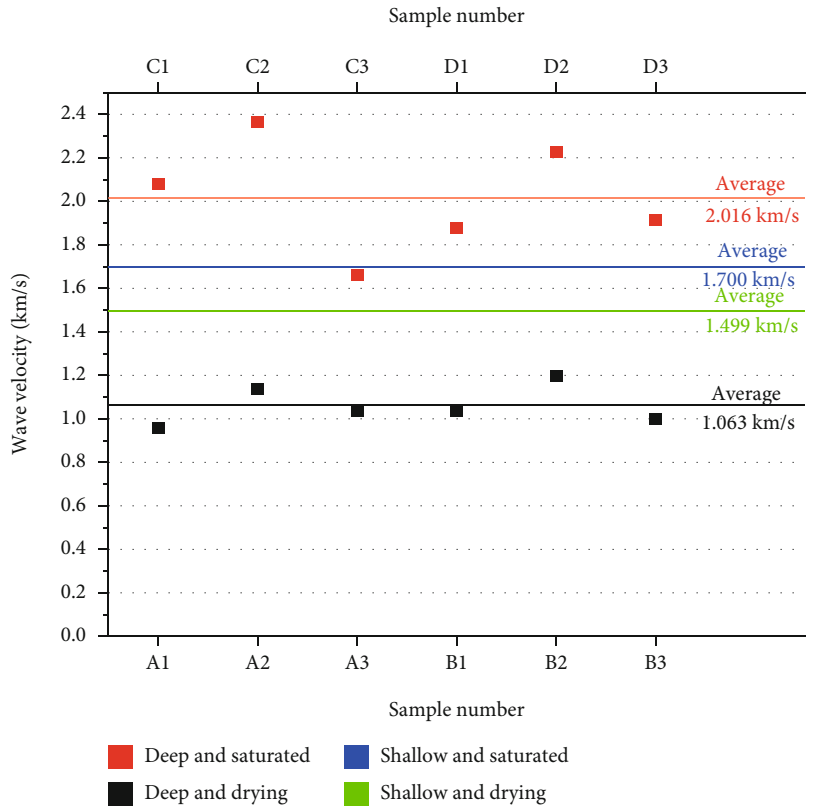

Figure 6: The wave velocity result of coal samples.

under different stress paths with drying and saturated conditions are shown in Figure 7 with obvious zoning characteristics.

On stress-strain curve of coal samples, the slope of liner connection between origin and the point of 50% compressive strength reflects the average stiffness of coal samples and characterizes the stability of the macro structure [43]. Compared with that of dry specimen under the same loading path, the average peak strength of deep saturated coal specimen under uniaxial compress path and uniaxial stepwise high stressed loading and unloading path decreased by 8.31% and 14.42%, respectively, and the average stiffness values decreased by 29.25% and 47.32%, respectively. It can be seen from the comparison that after the uniaxial stepwise high stressed loading and unloading path (imitating the repeated disturbance of deep coal) is applied in the elastic stage of the specimen, the strength and stiffness of deep coal samples are more affected, and after each stage of loading and unloading, the average stiffness of the specimen is almost a decrease of the linear weakening trend, as shown in Figure 8.

This is because under the uniaxial stepwise high stressed loading and unloading path, the existing cracks will continue to close and relax, and the new cracks will gradually sprout and develop. And some of them will cause irreversible damage to the coal structure. This damage accumulates with the increase of loading and unloading times and loading and unloading strength until the overall instability of the structure. It can be seen from Section 3.5 that water enters the deep coal mainly through the crack channel. And partial tension is given to intensify the deformation and interact with the hydrophilic material inside the coal sample so that the cohesive force between the particles is relatively weakened, which has a certain softening effect produced on the coal sample. As a result, the strength of coal samples decreases and the deformation increases, which leads to the gradual linear decrease of the bearing stiffness of the deep coal sample. In summary, the cracks in the deep coal specimens developed gradually are the root cause of the instability and failure of the coal specimens. The uniaxial stepwise high stressed loading and unloading path makes it easier for coal specimen to develop in the direction of crack propagation and structural instability. After the water enters the internal of coal sample specimens through these crack channels, the instability process of the deep coal specimens is also aggravated to a somewhat extent.

Previously, relevant scholars [37, 38] conducted uniaxial compression tests on coal sample specimens of No. 4 coal seam in Xishahe Coal Mine and coal sample specimens of No. 9 coal seam in Huangbaici Coal Mine. During the process of the moisture content of coal sample specimen of No. 4 coal seam in Xishahe Coal Mine increased from 0% to 5.29%, the average uniaxial compressive strength decreased from 23.21 MPa to 9.82 MPa by 57.69%, and the average peak strain increased from 0.011 to 0.023 by 109%. When the moisture content of coal sample specimen of No. 9 coal seam in Huangbaici Coal Mine increased from 0% to 5.67%, the average uniaxial compressive strength decreased from 16.48 MPa to 6.74 MPa by 59.10%, and the average peak strain increased from 0.013 to 0.026 by 100%. When the moisture content of coal sample

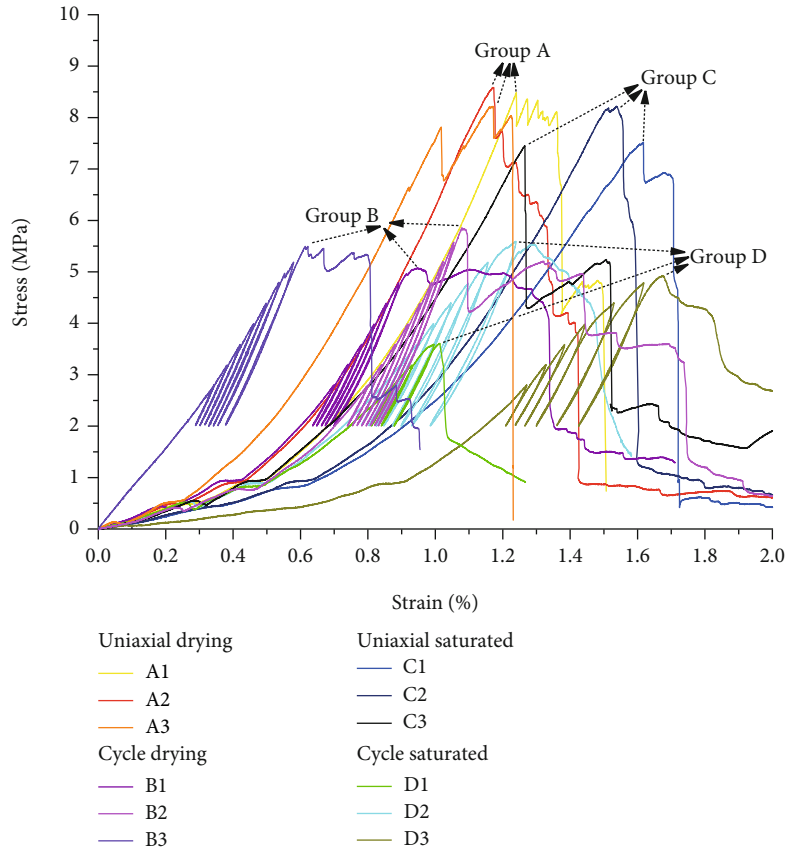

Figure 7: Stress-strain curve of deep coal samples.

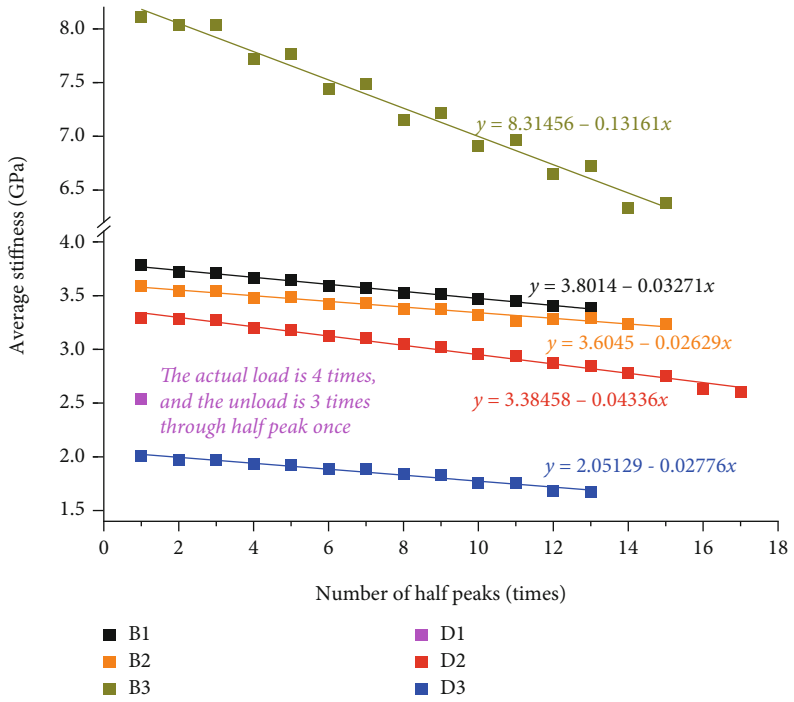

Figure 8: Relationship between average stiffness and cycle index of deep coal samples.

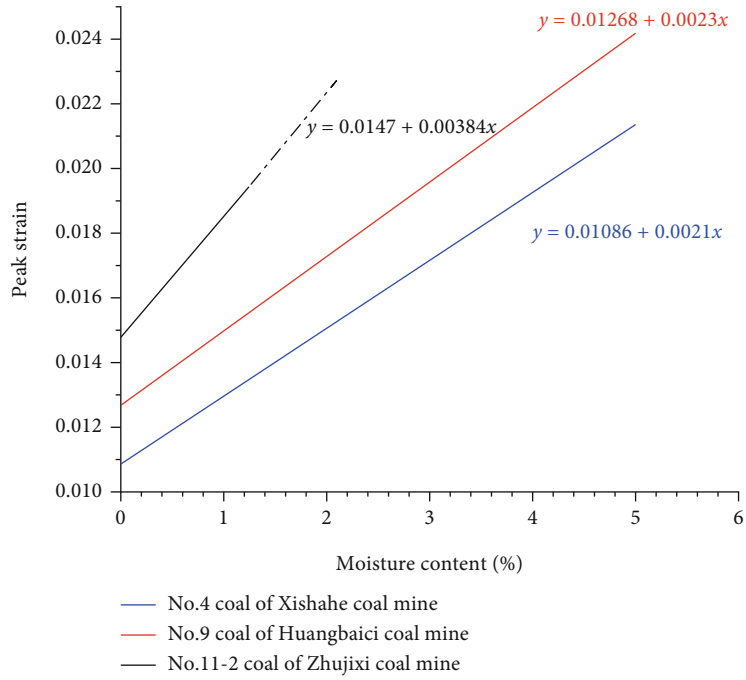

Figure 9: Relationship between peak stress and moisture content of coal sample.

specimen of 11-2 coal seam in Zhujixi Coal Mine increased from 0% to 1.25%, the average uniaxial compressive strength decreased from 8.58 MPa to 7.87 MPa by 8.31%, and the average peak strain increased from 0.0147 to 0.0195 by 23.29%, as shown in Figures 9 and 10.

Compared with the relatively shallow buried coal sample, the uniaxial compressive strength of the deep coal sample is lower. It can be seen from Section 3.2 that this is related to the great number of internal cracks under the initial state in deep coal body. But the whole skeleton structure of deep coal sample is denser, so the saturated water is less, and the weakening extent of water-rock interaction weakening is low. Therefore, under the condition of saturated water, the bearing strength of deep coal specimen with less moisture content decreases slightly.

In the process of mining and sampling, the more unloading amplitude of high stress confining pressure in deep coal is, more crack channels will be formed in the coal body. These cracks are more developed in quantity and volume than the relatively shallow buried coal samples. The water pressure in cracks can cause crack expansion, and the hydrodynamic pressure in cracks on coal and rock mass produced tangential thrust on coal [38, 39], which intensifies the deformation. Therefore, the expansion deformation properties of deep coal samples with more cracked water are more obvious.

3.5. Energy Density Distribution Characteristics of Deep Coal Samples. Assuming that there is no heat exchange during the instability of coal specimens, acoustic emission energy and radiation energy are ignored. According to the first law of thermodynamics, the energy density indexes of each stage before instability can be expressed as U_{ii}, U_{ei}, U_{di}, U_{ci}, and U_{pi}, which represents input energy density, elastic energy density, dissipation energy density, compress energy density, and plastic energy density in each stage, respectively, as shown in Figure 11.

In the initial compression stage (hereinafter referred to as the 0th cycle stage), there are only loading paths but no unloading paths. During this stage, the total input energy density U_{i0} is increasing continuously, which is stored in the specimen in the form of elastic energy density U_{e0}, and the dissipated energy density U_{d0} is dissipated in the form of plastic energy density U_{p0}, where cracks and pores are compressed. The calculation formula is as follows:

$$U_{i0} = \int_0^{\varepsilon_0} \sigma_0 d\varepsilon, \tag{2}$$

$$U_{e0} = \frac{1}{2}\left(\varepsilon_0 - \varepsilon_0'\right)\sigma_0, \tag{3}$$

$$U_{d0} = U_{i0} - U_{e0}. \tag{4}$$

In the loading stage of each small cycle in the high-stress stepwise loading and unloading stage (hereinafter referred to as the "i" cycle stage). Part of the input energy density U_{ii} is stored in the form of elastic energy density U_{ei}, and the other part is dissipated in the form of repeated compression energy density U_{ci} by compressing the plasticity of some cracks and pores in the previous cycle stage. In the unloading stage of each small cycle, the stored elastic energy density is released, and the dissipation energy density U_{di} is expressed in the form of cracks in the weak area of the coal structure. According to the study [8], the dissipation energy should be deducted from the U_{ci+1} compression energy value (hysteresis loop area) formed by the dense crack in the next loading process; it is

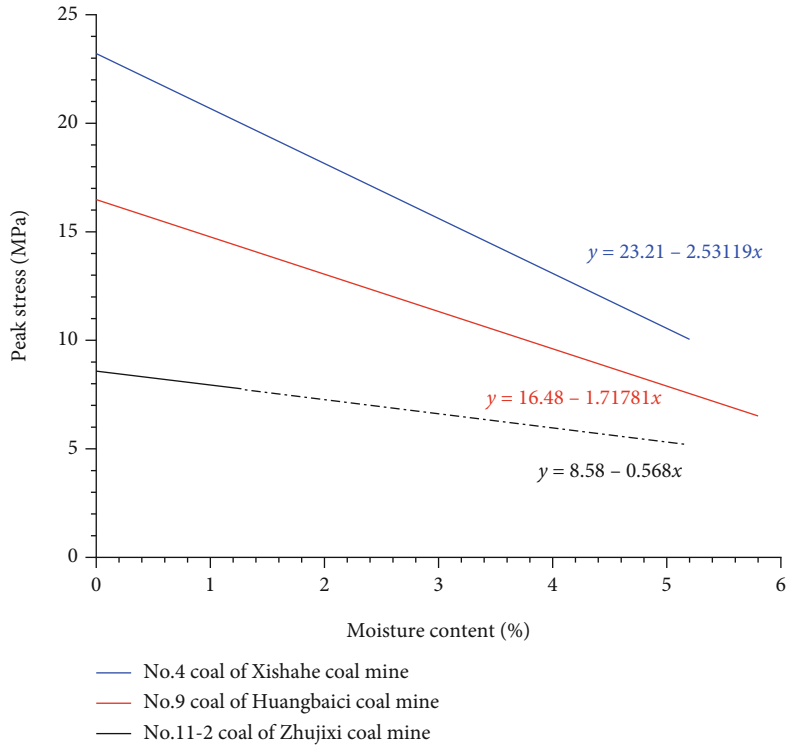

Figure 10: Relationship between peak strain and moisture content of coal sample.

the energy used to produce real damage in this cycle, which is called the plastic energy density U_{pi}. In the whole high-stress stepwise loading and unloading stage, the plastic energy density $U_{p1+2+\cdots+i}$ superimposed dissipation, causing damage accumulation of the specimen until the specimen enters the loading failure stage. The calculation formula is as follows:

$$U_{ii} = \int_{\varepsilon'_i}^{\varepsilon_i} \sigma_{0-i} d\varepsilon, \tag{5}$$

$$U_{ei} = \int_{\varepsilon'_{i+1}}^{\varepsilon_i} \sigma_{0-i} d\varepsilon, \tag{6}$$

$$U_{ci} = \int_{\varepsilon'_{i+1}}^{\varepsilon_{ci}} \sigma_{0-ci} d\varepsilon, \tag{7}$$

$$U_{di} = U_{ii} - U_{ei}, \tag{8}$$

$$U_{pi} = U_{ii} - U_{ei} - U_{ci}. \tag{9}$$

In the loading failure stage (hereinafter referred to as the final value "t" cycle stage), with the continuous input of energy and the continuous accumulation of damage, the energy storage density reaches the critical value, which is not enough to restore the input energy density U_{it} in this stage, and the specimen is unstable. Part of the energy causes the release of the plastic energy density U_{pt} of the specimen to produce macroscopic decomposition cracks and decomposes the coal sample into a number of fragments with large length of side. The other part mainly gives the kinetic energy of the specimen in the form of elastic wave to release the elastic energy density U_{et} in the form of a number of small length of debris. The calculation formula is as follows:

$$U_{it} = \int_{\varepsilon'_t}^{\varepsilon_t} \sigma_{0-t} d\varepsilon, \tag{10}$$

$$U_{et} = \frac{1}{2}\left(\varepsilon_t - \varepsilon'_t\right)\left(\sigma_t + \sigma'_t\right), \tag{11}$$

$$U_{dt} = U_{pt} = U_{it} - U_{et}. \tag{12}$$

The energy density of each specimen is calculated according to the calculation formula in this section. It is found that the input energy density of the deep coal sample in the initial compression stage is between $0.25383 * 10^4$ J/m^3 and $0.6736 * 10^4$ J/m^3, which is basically in a level of energy. After experiencing the drying-saturation conditions and different stress paths, the difference of energy density among the samples was gradually amplified but had a somewhat correlation. The relationship between energy density and stage cumulative loading press value of deep drying coal sample B1 and deep saturated coal sample D3 at each stage were plotted, as shown in Figures 12 and 13. The meaning of stage cumulative loading press value is that the cumulative value of pressure applied at each step loading stage. There are some similar laws to previous conventional cyclic loading and unloading tests of sandstone [44].

It can be seen from the diagram that the input energy density increases in each little cycle stage after the initial compression stage regardless of whether the deep coal sample is saturated or not until it enters the loading failure stage. The elastic energy density basically shows a linear upward

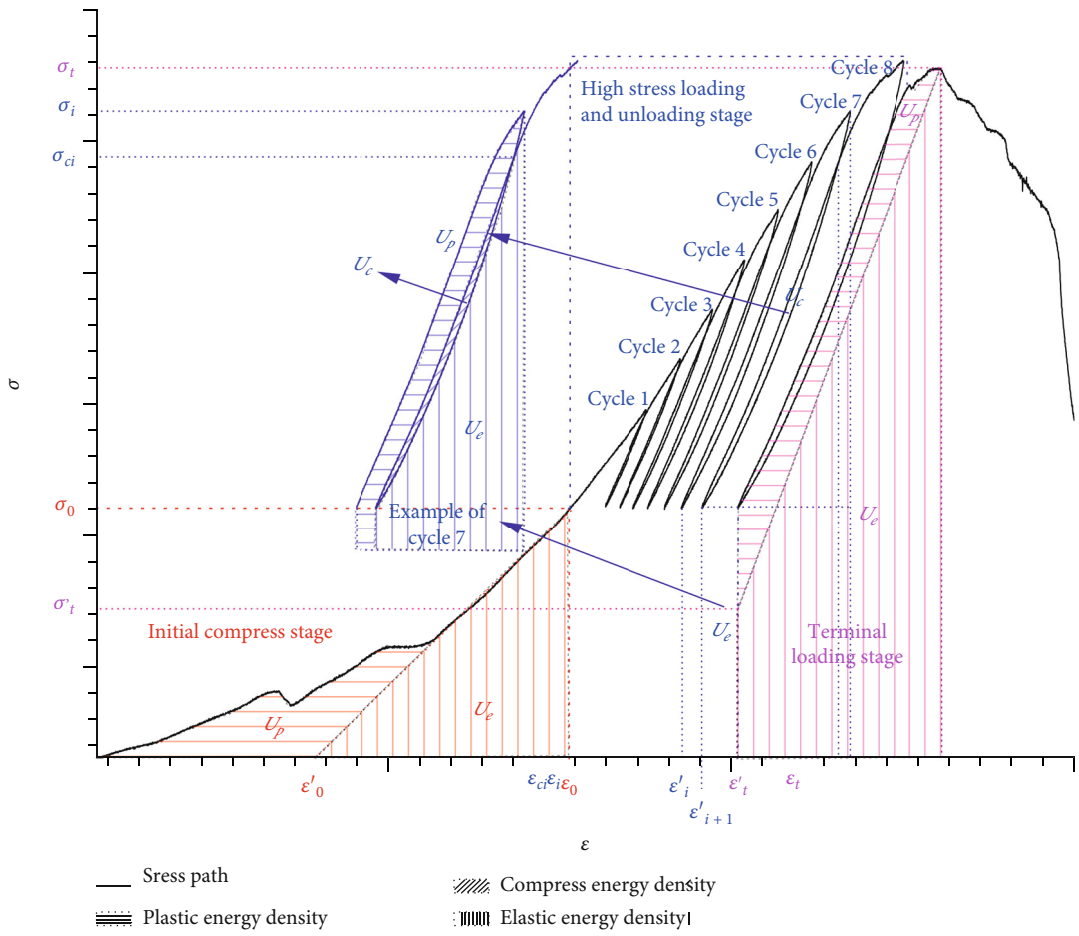

Figure 11: Diagram of energy density distribution of coal samples.

trend at each small cycle stage, and its energy density is always higher than dissipative energy. The dissipative energy density and plastic energy density showed a downward trend in the first two small cycles, but it increased steadily from the third small cycle until it entered the loading failure stage. The compression energy density showed a linear growth trend in the cyclic stage and returned to zero due to the absence of unloading path at the loading failure stage.

The relationship between energy proportion and stage cumulative loading press value for each stage of deep drying coal sample B1 and deep saturated coal sample D3 is shown in Figures 14 and 15. There are some similar laws to previous conventional cyclic loading and unloading tests of sandstone [44].

According to the energy proportion trend in the high stress of loading and unloading stage, whether the specimen is saturated or not, the development trend of energy proportion is basically positive and inverted "U" distribution. The longer stress course loaded, the more obvious these distribution characteristics are. The ratio of elastic energy density to input energy density presents an inverted "U" shape distribution with the increase of stress courses, and within one to two cycles before entering the loading failure stage, the ratio shows a significant downward trend. After entering the loading failure stage, the ratio rises rapidly again. As loading goes on, the instability failure of the specimen releases a large amount of elastic energy. The ratio of compress energy density and plastic energy density to total input energy density shows a positive "U" distribution with the increase of stress courses. And the ratio shows a significant upward trend in one to two cycles before entering the loading failure stage. A large number of cracks are developed in this part of the cycle, but the main structure still has a certain bearing capacity. The ratio of compression energy density to total input energy density shows an increasing trend in the high stress of loading and unloading stage, and it starts to show a relatively small downward trend until one to two cycles before loading failure. In the loading failure stage, the ratio returns to zero due to the absence of unloading path. The ratio of plastic energy density to dissipation energy density basically showed a downward trend in the early and middle stages of the high stress of loading and unloading stage and increased in the late stage of this cycle stage, indicating that the proportion of energy used to compress the original crack in the dissipation energy is decreasing. While the proportion of energy used to generate new cracks is increasing, the ratio of compression energy density to dissipation energy density is on the contrary. This law can also be used as a feature to determine the imminent failure of specimens.

Previously, Tang [28] carried out the energy density analysis of No. 3-1 coal (buried depth is about 400 meters, and the average saturated moisture content is 10.27%) in Chahasu

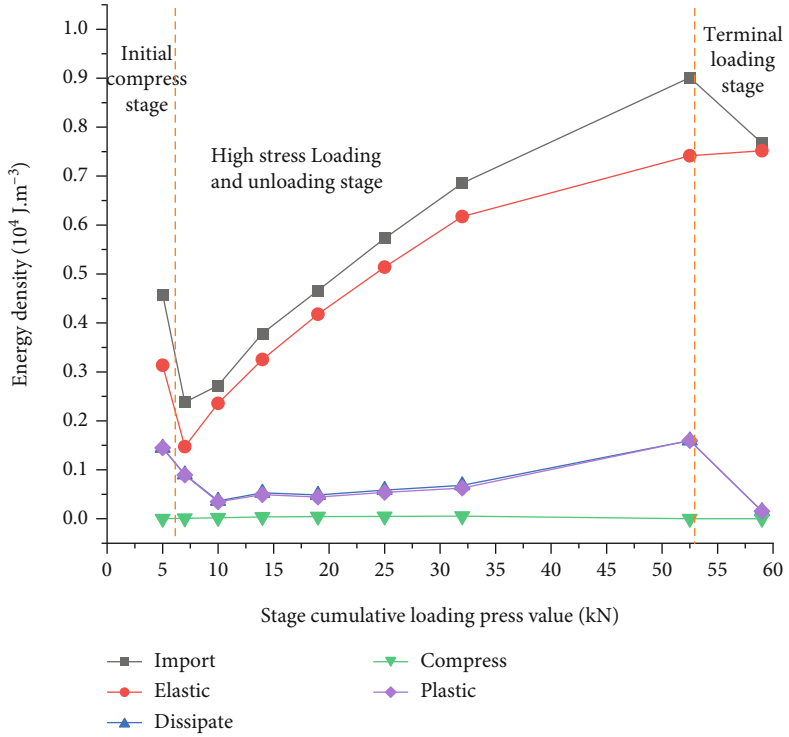

Figure 12: Relationship between energy density and stage cumulative loading press value with sample B1.

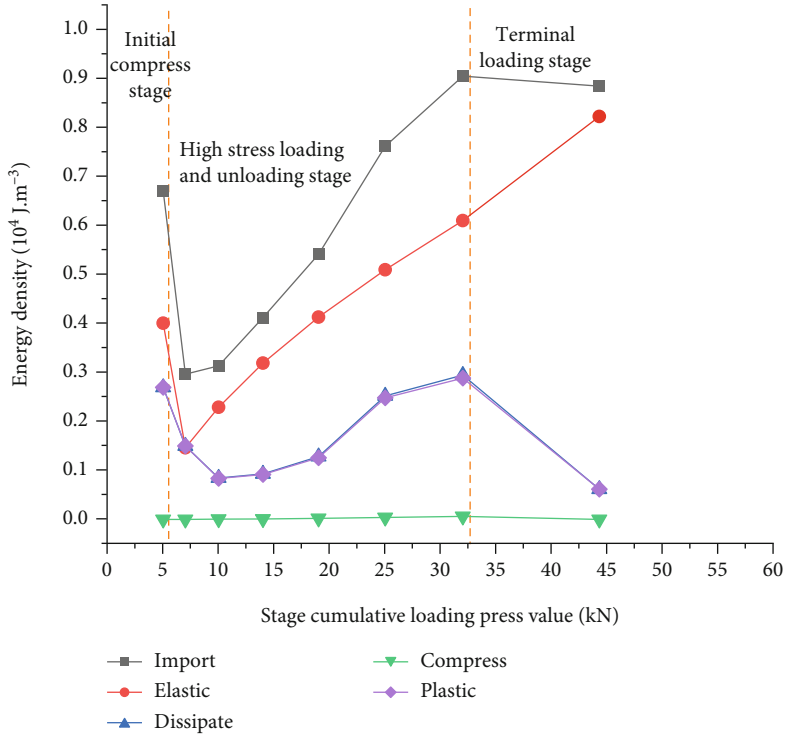

Figure 13: Relationship between energy density and stage cumulative loading press value with sample D3.

Coal Mine under uniaxial compression path. The energy density indexes of saturated shallow buried coal samples are lower than those of drying shallow buried coal samples in different degrees. The input energy density decreases by 53.6% from 140 kJ/m^3 to 65 kJ/m^3, and the elastic energy density decreases by 61.8% from 110 kJ/m^3 to 42 kJ/m^3, and the dissipation energy density decreased by 23.3% from 30 kJ/m^3 to 23 kJ/m^3. Under the uniaxial compress path of this test, the energy density index of saturated deep coal sample showed an upward trend compared with the same parameter index of drying deep

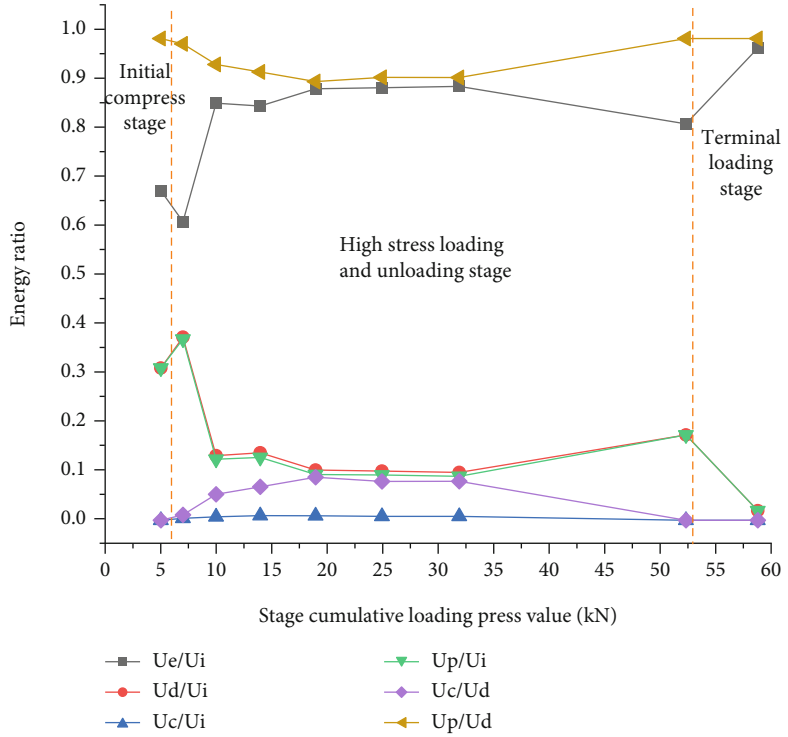

Figure 14: Relationship between energy proportion and stage cumulative loading press value with sample B1.

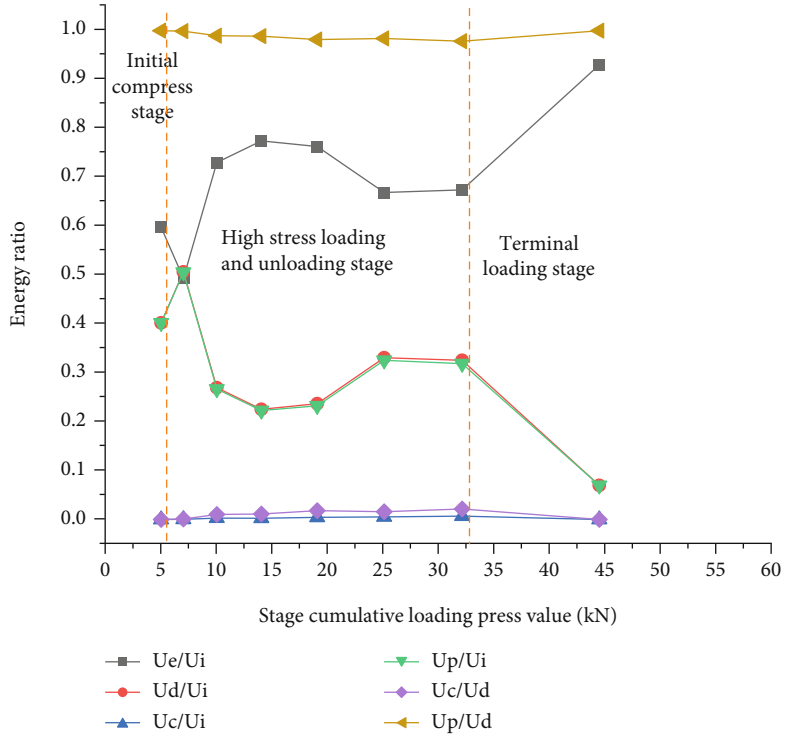

Figure 15: Relationship between energy proportion and stage cumulative loading press value with sample D3.

coal sample. The input energy density increased by 46.93% from 32.15 kJ/m^3 to 47.24 kJ/m^3, the elastic energy density increased by 17.6% from 25.93 kJ/m^3 to 30.50 kJ/m^3 by 17.6%, and the dissipation energy density increased by 33.10% from 6.22 kJ/m^3 to 8.28 kJ/m^3. From the analysis in Section 3.4, it can be seen that the uniaxial compressive strength of the deep coal specimen decreases slightly and the strain increases greatly after being saturated. Therefore, the energy index values of the deep coal sample basically show an upward trend, different from the relatively shallow buried coal samples.

Table 2: Table of scale reference range.

Category	Long edge range (mm)	Equivalent edge length value (mm)	Measurement method
Particles	<0.15	0.15	After screening, overall weighing, take the equivalent side length
	0.15-0.30	0.30	
	0.30-0.70	0.70	
	0.70-1.00	1.00	
	1.00-5.00	5.00	
Small block	5.00-10.00	10.00	After screening, one-by-one weighing, take the equivalent side length
	10.00-20.00	20.00	
	20.00-30.00	30.00	
Middle block	30.00-70.00	According to actual values	
Big block	>70.00	According to actual values	

On the whole, no matter whether the specimen is saturated or not, deep coal samples need less energy per unit volume failure destruction. The reason is that the original confining pressure of deep coal is larger, the amplitude and number of stress unloading in the mining process are more, and the initial cracks in the specimen are more and the injury degree is higher, resulting in lower peak stress and shorter loading process. Compared with the relatively shallow buried coal samples, the energy density is lower.

3.6. Mass Fractal Characteristics of Deep Coal Samples. The fragment of specimen is the process from microscopic damage to macroscopic fragmentation is the result of energy action and has mass fractal properties [45]. Therefore, the mass fractal experiment of deep coal samples has guiding significance for understanding its bearing properties. Combine the classification method of References [29, 46] with existing equipment, the fragment of the experiment is divided into 10 groups, as shown in Table 2, and the preliminary screening result is shown in Figure 16.

In this paper, the fractal dimension D of coal samples is calculated by using the correlation of mass (M)-equivalent edge length (L_{eq}) of fragments. The calculation formula is as follows:

$$L_{eqi} = 1000 * \sqrt[3]{m_i/1000/\rho/1000}, \tag{13}$$

$$\frac{M_{L_{eq}}}{M} = \left(\frac{L_{eq}}{L}\right)^k. \tag{14}$$

Taking logarithms on both sides of Equation (13), we simplify it to obtain

$$\lg\left(\frac{M_{L_{eq}}}{M}\right) = k \lg L_{eq} - k \lg L, \tag{15}$$

$$D = 3 - k. \tag{16}$$

In the formula, m_i is the mass of the first piece fragment, ρ is the average density of the coal sample, and L_{eqi} is the equivalent edge length of the "i" piece test block. After the calculation results are divided into the corresponding interval of equivalent edge length (L_{eq}), m_{Leq} is the cumulative mass of fragments within the range of L_{eq}, M is the total mass of all fragments involved in the calculation, and L is the correlation amount related to the average size; k is the slope of $\lg(M_{Leq}/M) - \lg L_{eq}$ under logarithmic coordinates.

According to the formula in this section, the $\lg(M_{Leq}/M)$ and $\lg(L_{eq})$ data of this experiment are obtained, and relevant fitting curves are made as shown in Figure 17. It can be seen that $\lg(M_{Leq}/M)$ and $\lg(L_{eq})$ have a strong linear correlation, indicating that the fragmentation mass distribution of deep coal samples after crushing has a good self-similarity, which is a fractal distribution with strong correlation [45], and the mass fractal dimension of this experimental sample is in the range of 1.69-1.95.

As shown in Figure 18, the mass fractal dimension D of deep coal specimen under the uniaxial stepwise high stressed loading and unloading path is smaller than that under uniaxial compression path. The reason is that the stepwise loading and unloading process of high stress aggravates the inside damage of the coal sample, resulting in the decrease of the bearing performance and energy storage property of the coal sample. In the loading failure stage with the largest number of microparticles and macrocracks generated, the elastic energy density and plastic energy density of the deep coal specimen are obviously smaller than those corresponding indexes under the uniaxial compression path after the uniaxial stepwise high stressed loading and unloading path, resulting in the reduction of the microparticles generated during the failure and the cracks used to divide the main body of the specimen, which makes it easier to form large-sized blocks. The decrease of the proportion of microparticles and the increase of the proportion of large-sized blocks lead to the decrease of the mass fractal dimension D under this loading path.

Under different loading paths, the fractal dimension of deep coal samples also shows a slightly downward trend after being subjected to saturated water, and the fractal dimension difference between saturated specimens is smaller than that of drying specimens. From the analysis in Section 3.2, it can be seen that the saturated water in the deep coal sample specimen is mainly filled in cracks, resulting in a certain saturated

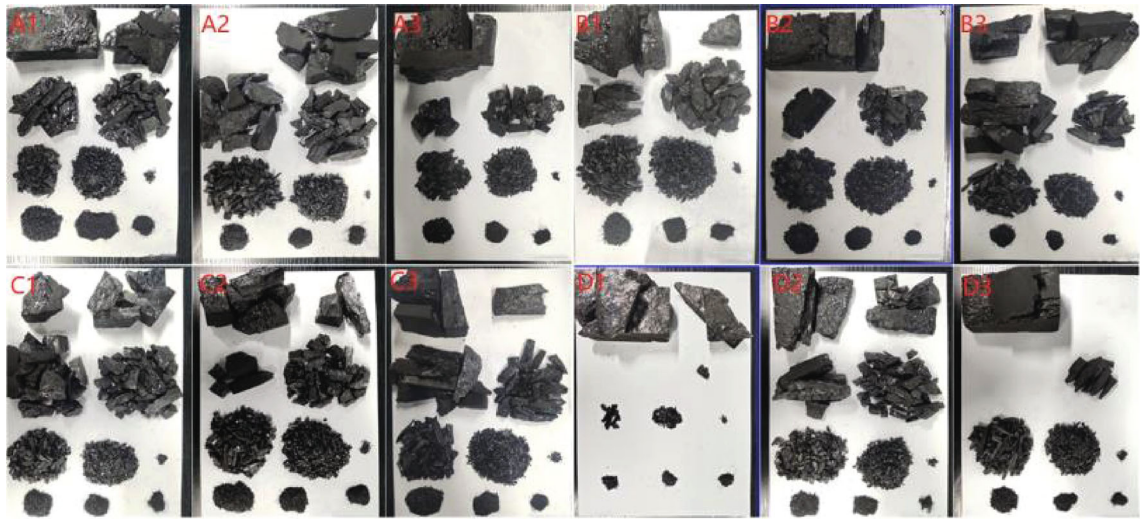

Figure 16: Initial screening and classification of specimen fragments.

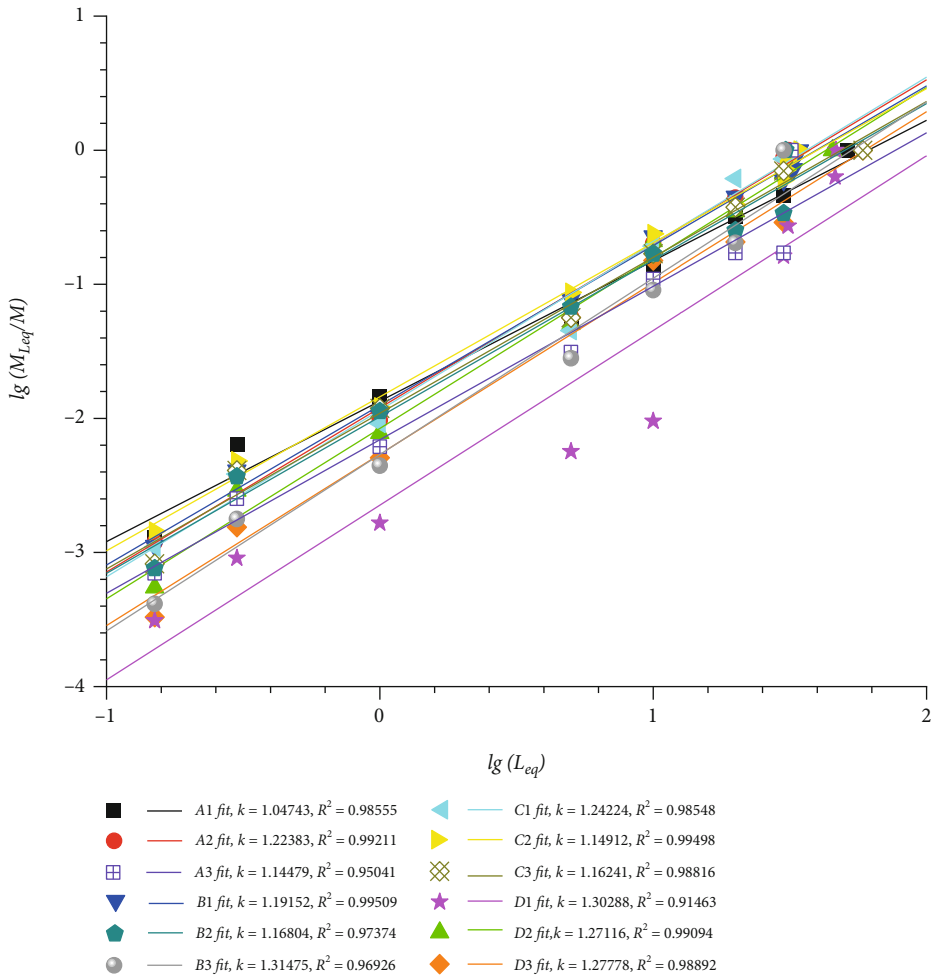

Figure 17: Logarithmic plot of equivalent length quality of coal sample pieces.

water pressure of crack [28, 38, 39], which makes it easier to transfer the stress of the specimen under load to the weak surface so that continue to develop and destroy, resulting in fewer new weak surfaces or new cracks. Therefore, the proportion of large-sized blocks is more, the proportion of small-size particles is less, and the fractal dimension D of saturated coal samples decreases after crushing. Saturated water also plays a static dissolution and dynamic material migration to a certain

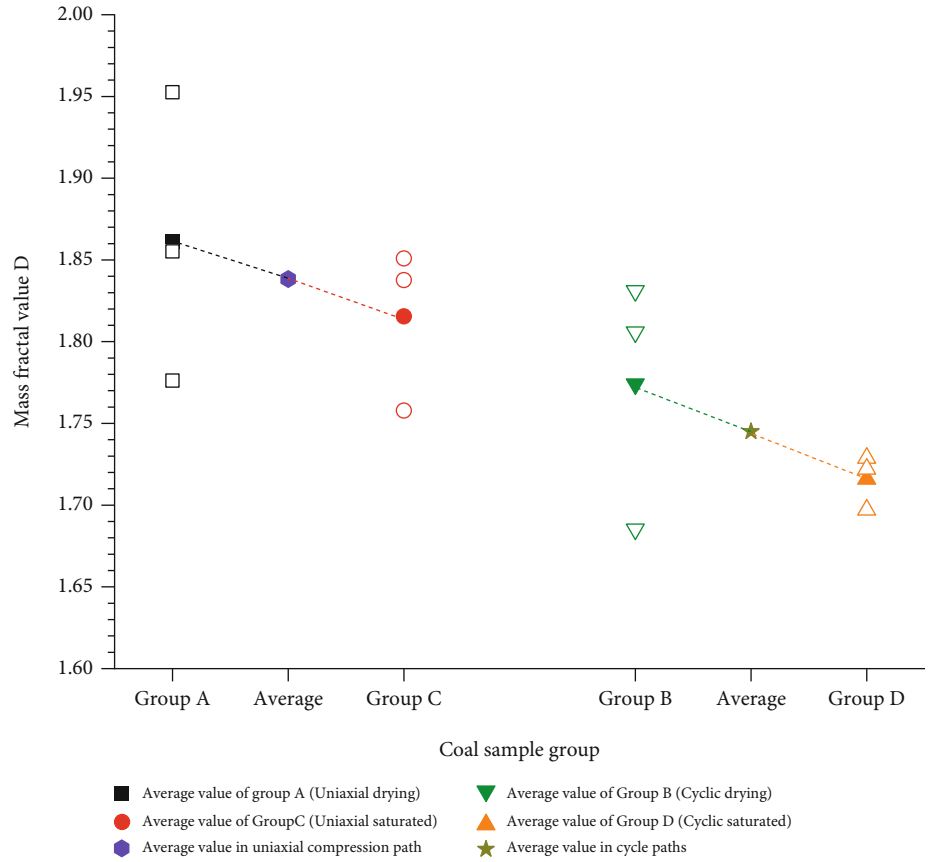

Figure 18: Mass fractal dimension distribution of coal sample.

extent [28, 38, 39], which increases the overall uniformity of coal samples to somewhat extent. Therefore, under the action of saturated water, the difference in the fractal dimension D of deep coal samples also decreases to a certain extent. However, the moisture content of deep coal specimens is low, so this decreasing trend is only to a small extent.

Previously, some scholars [30–32] have done some researches on the mass fractal of coal specimens with relatively shallow buried depth, and the fractal dimension is between 1.92 and 2.34, which is obviously bigger than the mass fractal dimension of deep coal samples in this experiment. In this experiment, the destruction of deep coal samples is mainly divided into large-scale fragments by producing few macro cracks, not needing too much stress loading and energy input, which well verifies the characteristics of weak bearing capacity and low energy density of the deep coal samples in Sections 3.4 and 3.5. It also indirectly shows that the structural characteristics of the deep coal samples are more influenced by cracks than the coal samples of relatively shallow buried depth.

3.7. Actual Occurrence Analysis of Deep Coal. The deep coal samples selected in this experiment are mechanical experimental specimens without obvious macro cracks in accordance with the requirements of the experimental specifications [32–35]. The deep coal samples located within a certain range of loose circles around the roadway may be closer to the eliminated specimens with obvious cracks shown in Figure 5. The saturated moisture content and uniaxial compressive strength are 4.05%, 0.94 MPa and 5.6%, 1.07 MPa, respectively. Compared with the mechanical experimental coal samples, the saturated water rate increases greatly and the bearing capacity decreases greatly. Therefore, in the actual mining process of deep mining, it is very important to control the crack development of deep coal. On the one hand, it can be optimized from the source of design to reduce the high-stress and space-time disturbance of repeated superposition of coal around the roadway and slow down the generation and development of cracks in coal. On the other hand, the support scheme can be optimized to control the crack expansion of deep coal and injecting some composite functional materials at suitable pressure with water resistance and reinforcement in time to control the continuous expansion of cracks, delaying the deterioration process of deep coal body under high stress disturbance and the action of "water-rock."

4. Conclusions

(1) Compared with the coal sample of relatively shallow burial depth, the deep coal sample has low moisture content and short water absorption process. The relative index value of the average rising rate of the ratio of water absorption in one stage to the total water absorption in the whole process is used to quantitative divide the threshold ranges of the fast,

slow, and saturated water absorption stages, which are 0.5-1%/h, 1-5%/h, and 5-100%/h, respectively

(2) The gradual development of cracks in the coal body is the root cause of the instability of the coal sample. Water enters the coal body through these cracks to aggravate the instability process, and the uniaxial stepwise high stressed loading and unloading path similar to the deep mining process makes the coal sample easier to develop in the direction of crack breeding. After each loading and unloading, the average stiffness value characterizing the macroscopic stability of the specimen is similar to the linear weakening trend

(3) Different from the coal samples with relatively shallow burial depth, the energy density indexes of the saturated deep coal samples are higher than those of the drying ones. However, in the high stress of loading and unloading stage, the overall trend of each energy proportion is similar to positive and inverted "U" distribution. The ratio of plastic energy to dissipation energy shows a downward trend in the early and middle stages of loading and unloading and increases in the late stage of loading and unloading, indicating that the energy proportion of the dissipation used to compress the original crack is decreasing, and the energy proportion used to generate new cracks is increasing. The ratio trend of compression energy to dissipation energy is opposite, which can be used as a feature to determine the imminent instability of deep coal

(4) Compared with the coal samples of relatively shallow burial depth, the elastic energy density and plastic energy density of the deep coal samples in the loading failure stage are at a low level, resulting in the smaller mass of small-sized particles generated by the release of elastic energy and the smaller number of cracks generated by the dissipation of plastic energy in the segmented specimens, mainly forming blocks with larger length and mass. Therefore, the mass fractal dimension of the deep coal samples is significantly smaller than that of the coal samples with relatively shallow burial depth in the previous studies

Data Availability

No data were used to support this study.

Conflicts of Interest

The authors declare no conflict of interest.

Acknowledgments

We are grateful to the China University of Mining and Technology for providing us with the research platform. The research described in this paper was financially supported by the National Natural Science Foundation of China (51874283).

References

[1] X. Li, S. Chen, S. Wang, M. Zhao, and H. Liu, "Study on in situ stress distribution law of the deep mine: taking Linyi mining area as an example," *Advances in Materials Science and Engineering*, vol. 2021, Article ID 5594181, 11 pages, 2021.

[2] Q. Guo, F. H. Ren, and Z. C. Zhang, "Stabality analysis of deep roadway based on coupled thermo-hydro-mechanical behaviors," *Advanced Materials Research*, vol. 594-597, pp. 2564–2568, 2012.

[3] S. Wang, Z. Xiang, J. Deng, H. Yang, X. Yang, and S. Jin, "Analysis of cooperative control effect of pressure relief and long bolt support for deep roadway under strong mining disturbance of adjacent working face," *Geotechnical and Geological Engineering*, vol. 39, pp. 2259–2268, 2021.

[4] L. Yuan, "Research progress of mining response and disaster prevention and control in deep coal mines," *Journal of China Coal Society*, vol. 46, no. 3, pp. 716–725, 2021.

[5] C. Hu, X. Yang, R. Huang, and X. Ma, "Presplitting blasting the roof strata to control large deformation in the deep mine roadway," *Advances in Civil Engineering*, vol. 2020, Article ID 8886991, 15 pages, 2020.

[6] C. Zheng, M. S. Kizil, Z. Chen, and S. M. Aminossadati, "Role of multi-seam interaction on gas drainage engineering design for mining safety and environmental benefits: linking coal damage to permeability variation," *Process Safety and Environmental Protection*, vol. 114, pp. 310–322, 2018.

[7] H. Yang, C. Han, N. Zhang, C. Sun, D. Pan, and M. Dong, "Stability control of a goaf-side roadway under the mining disturbance of an adjacent coal working face in an underground mine," *Sustainability*, vol. 11, no. 22, p. 6398, 2019.

[8] F. K. Xiao, Z. L. Shen, G. Liu, Z. Zhang, and F. R. Zhang, "Relationship between hysteresis loop and elastoplastic strain energy during cycle loading and unloading," *Chinese Journal of Rock Mechanics and Engineering*, vol. 33, no. 9, pp. 1791–1797, 2021.

[9] D. E. Hua-feng, F. A. Jing-cheng, L. I. Jian-lin, L. I. Guan-ye, Q. I. Yu, and X. U. Xiao-liang, "Damage evolution of dynamic characteristics of sandstone under the sequential action of water-rock interaction and cyclic loading and unloading," *Rock and Soil Mechanics (China)*, vol. 42, no. 2, pp. 343–351, 2021.

[10] X. Liu, X. Wang, E. Wang, Z. Liu, and X. Xu, "Study on ultrasonic response to mechanical structure of coal under loading and unloading condition," *Shock and Vibration*, vol. 2017, Article ID 7643451, 12 pages, 2017.

[11] S. Zhili, J. Shengguo, X. Wenbing, and T. Qingteng, "Research on coal acoustic emission characteristics and damage evolution during cyclic loading," *Frontiers in Earth Science*, vol. 10, article 818452, pp. 1–13, 2022.

[12] J. Chen, P. Liu, L. Liu et al., "Anchorage performance of a modified cable anchor subjected to different joint opening conditions," *Construction and Building Materials*, vol. 336, article 127558, 2022.

[13] J. Chen, Y. Zhao, H. Zhao, J. Zhang, C. Zhang, and D. Li, "Analytic study on the force transfer of full encapsulating rock bolts subjected to tensile force," *International Journal of Applied Mechanics*, vol. 13, no. 9, article 2150097, 2021.

[14] H. Guo, M. Ji, Y. Zhang, and M. Zhang, "Study of mechanical property of rock under uniaxial cyclic loading and unloading," *Advances in Civil Engineering*, vol. 2018, Article ID 1670180, 6 pages, 2018.

[15] F. Gong, J. Yan, S. Luo, and X. Li, "Investigation on the linear energy storage and dissipation laws of rock materials under uniaxial compression," *Rock Mechanics and Rock Engineering*, vol. 52, no. 11, pp. 4237–4255, 2019.

[16] W. Yang, H. Wang, Q. Zhuo et al., "Mechanism of water inhibiting gas outburst and the field experiment of coal seam infusion promoted by blasting," *Fuel*, vol. 251, pp. 383–393, 2019.

[17] W. A. Lianguo, M. I. Xiexing, W. U. Yu, S. U. Jian, and Y. A. Hongbo, "Discrimination conditions and process of water-resistant key strata," *Mining Science and Technology (China)*, vol. 20, no. 2, pp. 224–229, 2010.

[18] Y. Xue, J. Liu, X. Liang, S. Wang, and Z. Ma, "Ecological risk assessment of soil and water loss by thermal enhanced methane recovery: numerical study using two-phase flow simulation," *Journal of Cleaner Production*, vol. 334, p. 130183, 2022.

[19] Q. Yao, T. Chen, M. Ju, S. Liang, Y. Liu, and X. Li, "Effects of water intrusion on mechanical properties of and crack propagation in coal," *Rock Mechanics and Rock Engineering*, vol. 49, no. 12, pp. 4699–4709, 2016.

[20] Z. Lei, K. Zihao, X. Junhua, L. Mingxue, and Z. Cun, "Study on permeability law of intact and fractured coals under cyclic loading and unloading," *Chinese Journal of Rock Mechanics and Engineering*, vol. 40, pp. 2488–2499, 2021.

[21] X. Pengfei, D. Huafeng, Z. Hengbin et al., "Time-lag uniaxial compression failure characteristics of sandstone under different stress levels," *Rock and Soil Mechanics (China)*, vol. 42, pp. 3041–3050, 2021.

[22] Q. Meng, M. Zhang, Z. Zhang, L. Han, and H. Pu, "Experimental research on rock energy evolution under uniaxial cyclic loading and unloading compression," *Geotechnical Testing Journal*, vol. 41, no. 4, p. 20170233, 2018.

[23] C. Wang, B. He, X. Hou, J. Li, and L. Liu, "Stress–energy mechanism for rock failure evolution based on damage mechanics in hard rock," *Rock Mechanics and Rock Engineering*, vol. 53, pp. 1021–1037, 2020.

[24] Z. Jia, C. Li, R. Zhang et al., "Energy evolution of coal at different depths under unloading conditions," *Rock Mechanics and Rock Engineering*, vol. 52, no. 11, pp. 4637–4649, 2019.

[25] X. Y. Wang, H. W. Zhou, J. C. Zhong, L. Zhang, C. Wang, and L. An, "Study on energy evolution and permeability characteristics of deep coal damage under triaxial cyclic loading and unloading conditions," *Chinese Journal of Rock Mechanics and Engineering*, vol. 37, pp. 2676–2684, 2018.

[26] Q. B. Meng, C. K. Wang, B. X. Huang et al., "Rock energy evolution and distribution law under triaxial cyclic loading and unloading conditions," *Chinese Journal of Rock Mechanics and Engineering*, vol. 39, pp. 2047–2059, 2020.

[27] Y. Xue, J. Liu, P. G. Ranjith, Z. Zhang, F. Gao, and S. Wang, "Experimental investigation on the nonlinear characteristics of energy evolution and failure characteristics of coal under different gas pressures," *Bulletin of Engineering Geology and the Environment*, vol. 81, pp. 1–26, 2022.

[28] C. Tang, *Study on Damage Characteristics of Coal under the Influence of Dryness-Saturation Cycles and Acid Water Environment*, China University of Mining and Technology, MA thesis, 2020.

[29] Y. Y. Li, S. C. Zhang, Z. J. Wen et al., "Energy conversion and fragment distribution characteristics of coal sample under uniaxial cyclic loading," *Journal of China Coal Society*, vol. 44, pp. 1411–1420, 2019.

[30] H. Duan, *Study on the fatigue failure and fractal characteristics of coal subject to triaxial cyclic loading*, vol. 44, Shandong University of Science and Technology (China), PhD dissertation, 2018.

[31] H. P. Xie, F. Gao, and Y. Ju, "Research and development of rock mechanics in deep ground engineering," *Chinese Journal of Rock Mechanics and Engineering*, vol. 34, pp. 2161–2178, 2015.

[32] F. He, J. Dong, W. H. Liu, and Y. Xiong, *Regulation for Testing the Physical and Mechanical Properties of Rock-Part5: Test for Determining the Water Absorption of Rock*, Ministry of Land and Resources of the People's Republic of China, 2015.

[33] G. F. Zhao, L. Z. Liu, L. W. Cheng, and W. Y. Yi, *Regulation for Testing the Physical and Mechanical Properties of Rock-Part18: Test for Determing the Uniaxial Compressive Strength of Rock*, Ministry of Land and Resources of the People's Republic of China, 2015.

[34] Y. X. Mei, G. F. Zhao, J. Zeng, and L. W. Cheng, *Regulation for Testing the Physical and Mechanical Properties of Rock-Part19: Test for Determing the Deformability of Rock in Uniaxial Compression*, Ministry of Land and Resources of the People's Republic of China, 2015.

[35] R. Tan, L. Z. Liu, L. Z. Yuan, and B. F. Shi, *Regulation for Testing the Physical and Mechanical Properties of Rock-Part31: Test for Determining the Sound Velocity of Rock Mass*, Ministry of Land and Resources of the People's Republic of China, 2015.

[36] N. Chen, *Study on Damage Characteristics of Coal Pillar Dam Body of Groundwater Reservoir under Dynamic and Static Load*, China University of Mining and Technology, MA thesis, 2020.

[37] Q. L. Yao, W. N. Wang, X. H. Li, C. J. Tang, Q. Xu, and L. Q. Yu, "Study of mechanical properties and acoustic emission characteristics of coal measures under water-rock interaction," *Journal of China University of Mining and Technology*, vol. 50, pp. 558–569, 2021.

[38] B. Zhao, *Experimental Study on the Strength Weakening Characteristics of Coal Mass Subjected to Water Intrusion*, China University of Mining and Technology, MA thesis, 2014.

[39] C. Tang, Q. Yao, Z. Li, Y. Zhang, and M. Ju, "Experimental study of shear failure and crack propagation in water-bearing coal samples," *Energy Science & Engineering*, vol. 7, no. 5, pp. 2193–2204, 2019.

[40] C. Sun, G. Li, M. Elgharib Gomah, J. Xu, and H. Rong, "Meso-scale mechanical properties of mudstone investigated by nano-indentation," *Engineering Fracture Mechanics*, vol. 238, p. 107245, 2020.

[41] W. Gang, W. Shibin, L. Huaixing, Q. Xiangjie, and L. Shengpeng, "Study on water phase seepage evolution model considering mesoscale characteristics of pore and fissure in coal," *Chinese Journal of Rock Mechanics and Engineering*, vol. 40, pp. 1547–1558, 2021.

[42] Y. Xue, J. Liu, P. G. Ranjith, F. Gao, H. Xie, and J. Wang, "Changes in microstructure and mechanical properties of low-permeability coal induced by pulsating nitrogen fatigue fracturing tests," *Rock Mechanics and Rock Engineering*, vol. 22, pp. 1–20, 2022.

[43] L. I. Yage, J. I. Longzhe, and T. A. Hao, "Experiment of loading rate effect on mechanical characteristics of cemented filling

body," *Journal of Harbin Institute of Technology (China)*, vol. 48, pp. 49–53, 2016.

[44] X. Li, Z. Yao, X. Huang, Z. X. Liu, X. Zhao, and K. H. Mu, "Investigation of deformation and failure characteristics and energy evolution of sandstone under cyclic loading and unloading," *Rock and Soil Mechanics (China)*, vol. 42, no. 6, pp. 1693–1704, 2021.

[45] H. Xie, F. Gao, H. W. Zhou, and J. P. Zuo, "Fractal study of rock fracture and fracture," *Journal of Disaster Prevention and Mitigation Engineering (China)*, vol. 23, pp. 1–9, 2003.

[46] M. C. He, G. X. Yang, J. L. Miao, X. N. Jia, and T. T. Jiang, "Classification and research methods of rockburst experiment fragment," *Chinese Journal of Rock Mechanics and Engineering*, vol. 28, pp. 1521–1529, 2009.